ACS OMEGA

Open Access

http://pubs.acs.org/journal/acsodf

Article

Numerical Simulation Study on Combustion of Low Calorific Value Waste Blended with Biomass

Zhengguang Huang, Dehong Gong,* Changyang Peng, Jiandong Chen, Jie Luo, Yuanyuan Xu, and Lang Yang

Cite This: *ACS Omega* 2024, 9, 14297−14309

Read Online

ACCESS | Metrics & More | Article Recommendations

ABSTRACT: Numerical simulations of a 600 t/day waste incinerator was carried out using the fluid dynamic incinerator code and Fluent to evaluate the effect of biomass blending on furnace temperature, pollutant generation, and selective noncatalytic−reduction (SNCR) denitrification when treating low calorific−value waste. The results show that as the biomass blending ratio increases, the water content gradually decreases, the calorific value increases, and the maximum temperature of the incinerator gradually increases from 1227 to 1408 K, while the content of exported NO_x increases from 579 to 793 mg/Nm^3; during the combustion of low-quality waste, the residence time of the flue gas in the high-temperature region (above 1123 K) is 1.62 s. When the biomass blending ratio exceeds 20%, the residence time of the flue gas in the high-temperature region is more than 2 s, which can effectively curb the generation of dioxin. When the biomass blending ratio is 20%, and the normalized stoichiometric ratio ($2n_{urea}/n_{NO}$) of urea injected into the SNCR is 1.1, the NO_x concentration at the outlet is 230.08 mg/Nm^3, which satisfies the NO_x emission standard of less than 250 mg/Nm^3.

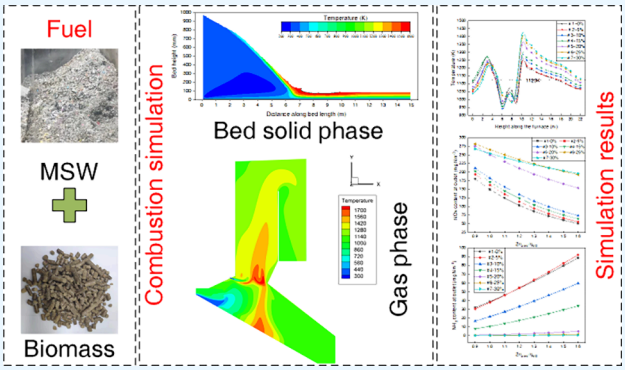

1. INTRODUCTION

With the development of China's economy and acceleration of urbanization, the amount of municipal solid waste removal has grown from 164 million tons in 2011 to 249 million tons in 2021,[1] indicating an increase of 51.68% in 10 years. At present, municipal solid waste is mainly treated in landfills and incineration. However, landfill has several drawbacks such as generation of leachate, greenhouse gas emissions, and utilization of land resources on a large scale.[2] Waste incineration−based power generation is considered as the world's most promising waste treatment technology.[3] However, the composition of municipal solid waste is complex, and the composition of the waste collected from different regions and in different seasons significantly varies, and the water content is also different.[4] Therefore, the actual operation of an incinerator involves unstable combustion at a low incinerator temperature, which cannot effectively curb the generation of dioxins. Further, the emission of NO_x is unstable, which seriously affects the operational efficiency of the unit.

Computational fluid dynamics is widely used to numerically simulate combustion processes in waste incinerators. Sun et al.[5] simulated the effect of waste particle size on the combustion process of a waste bed. Hoang et al.[6] used numerical simulations to evaluate the velocity-field, temperature-field, and component-field distributions of a waste incinerator. Wissing et al.[7] used the discrete element method to simulate the waste combustion process on a grate; they also utilized Fluent to study the combustion in a furnace chamber. Gu et al.[8] carried out numerical simulations of a 750 t/day waste incinerator to evaluate the effect of the changes in waste components and air distribution on combustion. Their results showed that changing the garbage components without changing the operational conditions led to an uneven temperature distribution, and adjusting the air distribution helped in improving the thermal efficiency of the boiler. Yan et al.[9] studied the effect of different primary air temperatures on the combustion characteristics of an incinerator through numerical simulations, and the results showed that as the primary air temperature increased, the rate of water evaporation and volatilization increased. However, the rate of volatilization was very high, which led to the localization of the

Received: December 18, 2023
Revised: January 28, 2024
Accepted: March 5, 2024
Published: March 14, 2024

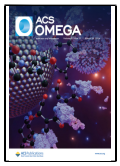

incinerator, and a high temperature was detected inside the incinerator.

During the incineration of municipal solid waste, other solid wastes are coprocessed as well. Yang et al.[10] employed a 500 t/day waste incinerator and performed numerical simulations to investigate municipal waste mixed with high calorific−value waste during the combustion process as well as to evaluate the impact of the distribution of the field of different air supplies. The results showed that the maximum temperature for bed combustion remained unchanged under different ratios of primary air and the angle of secondary air injection significantly influenced the gas flow in the incinerator. Waste incineration coprocessing of other solid wastes not only changed the combustion characteristics but also affected the generation of pollutants. Zeng et al.[11] performed numerical simulations on a domestic waste incinerator mixed with domestic sludge and analyzed the sludge mixing amount, effect of sludge moisture content on incinerator combustion, and flow field and pollutant emission characteristics. Their results showed that as the sludge mixing amount increased, the water evaporation rate accelerated, the incinerator temperature decreased, and the NO_x emission was reduced. Hu et al.[12] simulated the selective noncatalytic−reduction (SNCR) denitrification process during the incineration of municipal waste in a waste incinerator, and the results showed that different SNCR injection positions, speeds, and normalized stoichiometric ratios only negligibly affected the incinerator temperature and O_2 concentration; the injection position significantly influenced the denitrification effect and NH_3 slip, the highest denitrification efficiency of 51.50% was achieved when the injection speed was 13.80 m/s, and the amount of NH_3 slipped was 11.08 mg/Nm^3.

As the fourth largest energy source after coal, petroleum, and natural gas, biomass is abundant, is widely distributed all over the world,[13] and exhibits a high calorific−value. Therefore, in this study, we performed numerical simulations to evaluate the flue-gas velocity-field, temperature-field distribution, and NO_x generation in a furnace during the combustion of low-calorific-value garbage mixed with biomass in a waste incinerator. We assessed the effect of normalized stoichiometric ratio on SNCR denitrification using a discrete phase model (DPM), which provided a theoretical support for waste-to-energy plants to stabilize combustion by blending biomass during the combustion of low-quality waste.

2. RESEARCH OBJECT

A waste incineration power plant with a 600 t/day grate furnace was adopted as the study target. The total grate length of 14.83 m was divided into three sections: the drying grate lengths of 3.61 m, the combustion grate length of 5.61 m, and the ashes combustion grate length of 5.61 m; the grate width was 7.02 m, and the grate inclination angle was 15°. The primary air was preheated by an air preheater through the grate located below six air chambers in the furnace chamber. The secondary air inlet was located at the top of the arch on the incinerator's front and throat of the upper part of the secondary air outlet. Cold air at a temperature of 20 °C passed through the furnace's structure as shown in Figure 1. The secondary air was fed by cold air (at 20 °C) passed through the secondary air outlet; the structure of the incinerator is illustrated in Figure 1, and the fuel characteristics of the garbage and biomass waste are shown in Table 1.

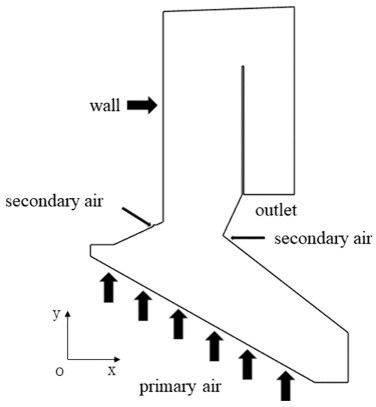

Figure 1. Structural model of a waste incinerator.

3. MATHEMATICAL MODEL AND BOUNDARY CONDITIONS

3.1. Model Assumptions.

1. The waste on the bed is regarded as a porous medium with the same particle size; the porosity remains constant throughout the combustion process, and the interior of the particles is regarded as isothermal and adiabatic.
2. The waste contains only moisture, volatile matter, fixed carbon, and ash, and the combustion process of the waste on the grate involves drying, volatile release, gas combustion, and coke combustion. The volatile analyzed gas is only composed of CH_4, CO, CO_2, and H_2O.
3. Only the change in the direction of waste movement in the grate and that in the direction of bed thickness are considered.
4. Particle crushing during the combustion as well as ash slagging and melting is ignored. Further, ideal gases and fly ash particles are considered, and the bed only includes the gas phase.

3.2. Mathematical Model. The combustion process of waste in the incinerator can be divided into bed solid-phase combustion and furnace gas-phase combustion. The bed solid-phase combustion is simulated by the fluid dynamic incinerator code (FLIC), a bed combustion simulation software is developed by Yang et al.[14] and the furnace gas-phase combustion is simulated by Fluent, which is used to obtain the parameters of flue-gas temperature, component, and velocity distribution in the upper part of the bed and then used as the inlet boundary condition of the furnace gas-phase combustion and the gas radiation obtained by Fluent as the radiation boundary condition of FLIC. After the calculation of furnace gas-phase combustion is completed, the gas radiation obtained from Fluent is used as the radiation boundary condition of FLIC, and the boundary conditions are iterated until convergence.

The refuse bed is considered as a porous medium structure, with the solid phase consisting of the refuse and the gas phase consisting of air-filled interrefuse pores.[15] The combustion of refuse on the grate was modeled using the combustion model of Yang et al.,[16] and the main equations for the solid phase of the bed are as follows:

Continuity equation

$$\frac{\partial}{\partial t}(\rho_s(1-\phi)) + \nabla \times (\rho_s(1-\phi)V_s) = S_s \quad (1)$$

https://doi.org/10.1021/acsomega.3c10104
ACS Omega 2024, 9, 14297−14309

Table 1. Industrial and Elemental Analyses of Wastes and Biomass

	industrial analysis (ar, %)				elemental analysis (daf, %)				
category	moisture	volatiles	stationary carbon	ash	C	H	O	N	S
MSW1	46.5	25.5	8	20	60.39	8.6	28.3	1.40	0.06
MSW2	56	18.27	5.73	20	59.38	8.42	29.58	1.46	0.04
biomass	11.99	71.52	5.49	10.98	38.31	6.06	51.37	3.39	0.88

where ϕ is the bed porosity; $\rho_s$is the solid-phase density, kg/m^3; V_s is the solid-phase velocity, m/s; S_s is the mass source term.

Momentum equation

$$\frac{\partial}{\partial t}(\rho_s(1-\phi)V_s) + \nabla \times (\rho_s(1-\phi)V_sV_s) + -\nabla \times \sigma - \nabla \times \tau + \rho_s(1-\phi)g + A \quad (2)$$

where σ is the normal stress tensor in the bed and τ is the tangential stress tensor in the bed; A is the random motion of particles.

Energy equation

$$\frac{\partial(\rho_s(1-\phi)H_s)}{\partial t} + \nabla \times (\rho_s(1-\phi)V_sH_s) = \nabla \times (\lambda_s \nabla T_s) + S_a h_s'(T_s - T_g) + \nabla \times q_r + Q_{sh} \quad (3)$$

where H_s is the solid-phase enthalpy; $T_s$is the solid temperature; Q_{sh} is the solid-phase heat source; $q_r$is the radiant heat flux; and λ_s is the effective thermal conductivity of the bed and $\lambda_s = \lambda_{s0} + \lambda_{sm}$ (λ_{s0} is the conductivity of the solid material, and λ_{sm} is the heat transfer caused by the random movement of the particles).

Transport equation

$$\frac{\partial(\rho_s(1-\phi)Y_{i,s})}{\partial t} + \nabla \times (\rho_s(1-\phi)V_sY_{i,s}) = \nabla \times (D_s\nabla(\rho_s(1-\phi)Y_{i,s})) + S_{Y_{i,s}} \quad (4)$$

The gas-phase combustion process simplifies the mixed gas analyzed via bed combustion volatilization into CH_4, CO, H_2O, and CO_2.[17] The gas-phase combustion adopts the finite rate/eddy dissipation model(FR/ED), and the combustion kinetic equation is as follows:

$$CH_4 + 0.5O_2 \rightarrow CO + 2H_2 \quad (5)$$

$$CH_4 + 1.5O_2 \rightarrow CO + 2H_2O \quad (6)$$

$$CO + 0.5O_2 \rightarrow CO_2 \quad (7)$$

Reaction speed

$$R_{CH_4} = 5.012 \times 10^{11} \times \exp\left(-\frac{2 \times 10^8}{RT_g}\right) \times C_{CH_4}^{0.7} \times C_{O_2}^{0.8} \quad (8)$$

$$R_{CO} = 2.239 \times 10^{12} \times \exp\left(-\frac{1.7 \times 10^5}{RT_g}\right) \times C_{CO} \times C_{O_2}^{0.25} \times C_{H_2O}^{0.5} \quad (9)$$

MSW incineration mainly produces fuel-based NO_x and thermal NO_x. Fuel-based NO_x generation is calculated using additional transport equations, whereas thermal NO_x is mainly produced by oxidation of N_2 at high temperatures and is described by the Zeldovich mechanism.[18]

$$N_2 + O \rightarrow N + NO \quad (10)$$

$$N + O_2 \rightarrow O + NO \quad (11)$$

$$N + OH \rightarrow H + NO \quad (12)$$

The thermal NO_x generation rate is expressed as

$$\frac{d[NO]}{dt} = 3 \times 10^{14}[N_2][O]^{1/2}\exp(-542000/RT) \quad (13)$$

The rate of fuel-based NO_x generation depends on the nitrogen content of the fuel and the local combustion temperature. Fuel nitrogen is released into the flue gas as HCN and other intermediates during combustion and is then converted to NO_x. We assume that the nitrogen in the fuel is converted to HCN intermediates in 55% of the fuel, 5% is converted to NH_3, and 40% is directly generated NO.[19]

SNCR denitrification uses a urea solution, and a DPM is used to describe the injection process.[20] The decomposition mechanism of urea solution is shown in Table 2,[21] and the reaction mechanism of SNCR denitrification is shown in Table 3.[22]

Table 2. Decomposition Mechanism of Urea Solution

reaction equation	A	b	E/(J/mol)
$CO(NH_2)_2 \rightarrow NH_3 + HNCO$	1.27×10^4	0	65048.109
$CO(NH_2)_2 + H_2O \rightarrow 2NH_3 + CO_2$	6.13×10^4	0	87819.133

Table 3. SNCR Denitrification Reaction Mechanism

reaction equation	A	b	E/(J/mol)
$NH_3 + NO \rightarrow N_2 + H_2O + H$	4.24×10^2	5.30	349937.06
$NH_3 + O_2 \rightarrow NO + H_2O + H$	3.50×10^{-1}	7.65	524487.005
$HNCO + M \rightarrow NCO + M + H$	2.40×10^8	0.85	284637.8
$HCO + NO \rightarrow N_2O + CO$	1.00×10^7	0.00	−1632.4815
$NCO + OH \rightarrow NO + CO + H$	1.00×10^7	0.00	0.00
$N_2O + OH \rightarrow N_2 + O_2 + H$	2.00×10^6	0.00	41858.5
$N_2O + M \rightarrow N_2 + O + M$	6.90×10^{17}	−2.50	271075.646

3.3. Calculation Methods and Boundary Conditions.

According to the actual size of the incinerator, the geometric model of the incinerator hearth part is established at a ratio of 1:1. Local encryption is carried out in the areas of intense combustion and large flue-gas disturbances, such as the secondary air outlet and upper area of the grate, and the final grid number is 3.45 million, whose grid independence is verified before the calculations. The gas-phase combustion of the furnace is simulated using a three-dimensional steady-state discrete model; the gas-phase turbulence simulation adopts the standard $k-\varepsilon$ model; the P1 model is used to simulate the radiative heat transfer; the combustion model is based on the finite rate/vortex dissipation model; the SIMPLE algorithm is selected for coupling the velocity and pressure; and the

https://doi.org/10.1021/acsomega.3c10104
ACS Omega 2024, 9, 14297−14309

second-order windward format is used for all the solved equations.

The amount of waste in the furnace is 600 t/day; the time of garbage on the grate is 1.75 h; the excess air coefficient is 1.3; the ratio of primary and secondary is 0.8:0.2; the ratio of six air chambers is 0.20:0.15:0.15:0.15:0.2:0.15; and the temperature of the primary air is 453 K. Before performing calculations for the mixing and combustion, ordinary garbage with a moisture content of 46.5% was used to numerically simulate and compare with field operation data to verify the reliability of the model's calculations. Then, numerical simulation of different biomass waste blending combustion was carried out for the high moisture−content garbage, and a total of eight working conditions were simulated, and the working condition parameters are shown in Table 4. The inlet and secondary

Table 4. Numerical Simulation of Working Conditions

	# 0%−0%	# 1%−0%	# 2%−5%	# 3%−10%	# 4%−15%	# 5%−20%	# 6%−25%	# 7%−30%
MSW moisture content/%	46.5	56	56	56	56	56	56	56
biomass blending ratio/%	0	0	5	10	15	20	25	30

air inlet are used with the velocity inlet, and the temperature of the secondary air is 293 K; the outlet is used with the pressure outlet boundary, and the pressure is −50 Pa.

SNCR denitrification uses a urea solution with a concentration of 10%. The SNCR injection position is shown in Figure 2. The urea mass−flow rate is calculated using eq 14. The droplet size in the urea solution follows the Rosin−Rammler distribution[23] and is in the range of 40−120 μm, with the average diameter being 60 μm. The expansion

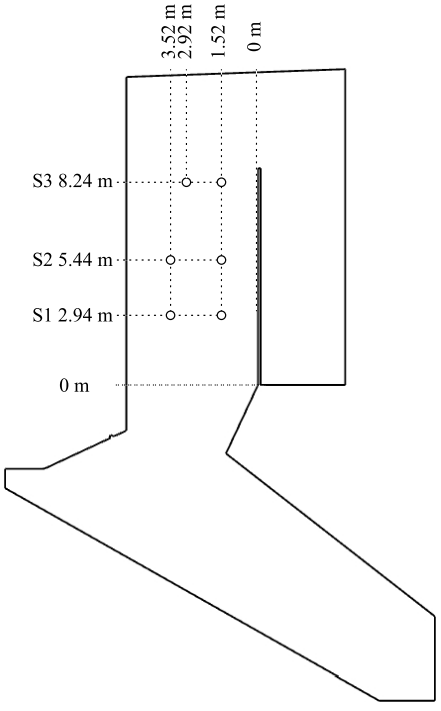

Figure 2. Schematic showing the SNCR ammonia injection position.

coefficient is 3.5; the solid cone injection method, with a cone angle of 30°, is used.[24]

$$Q_{urea} = \frac{Q_{NO}}{30} \times \frac{60}{2} \times N_{SR} \quad (14)$$

where Q_{urea} is the mass-flow rate of urea; Q_{NO} is the mass-flow rate of NO; N_{SR} is the normalized stoichiometric ratio ($2n_{urea}/n_{NO}$, n_{urea} is the number of moles of urea, n_{NO} is the number of moles of NO).

4. ANALYSIS AND DISCUSSION OF RESULTS

4.1. Model Verification. Municipal solid waste with a moisture content of 46.5% was used as the fuel, and the physical parameters of the waste are shown in Table 1. The bed combustion was simulated using FLIC, and the corresponding moisture evaporation, volatilization release, and fixed carbon combustion rates are shown in Figure 3.

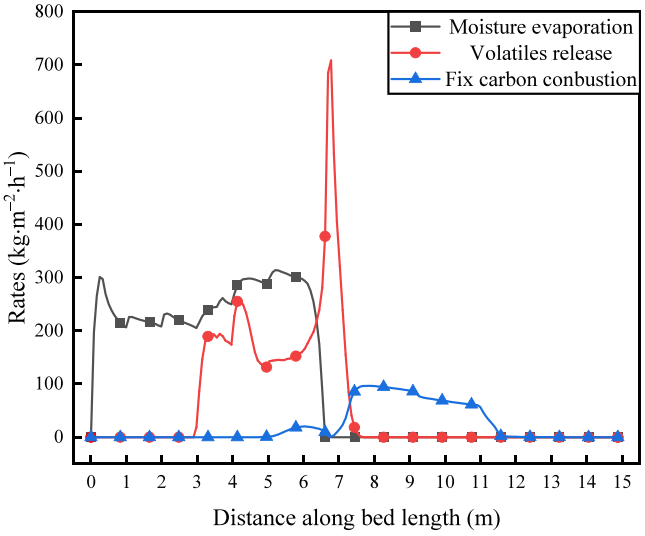

Figure 3. Chart of water evaporation, volatilization analysis, and fixed carbon burning rate along the direction of grate movement

Evidently, water evaporation occurs immediately after the garbage enters the drying grate under heat transfer by the primary air and furnace's flue gas, and owing to the high moisture−content of the garbage, water evaporation takes a long time and is completed in the middle of the combustion grate (about 6.5 m). The volatile fraction starts to precipitate at the end of the drying grate (around 3 m); the peak of the precipitation rate occurs at ∼6.7 m, after which the precipitation rate decreases rapidly to zero, and volatile precipitation is completed. The combustion of fixed carbon starts at ∼5 m. At ∼6.7 m, due to the precipitation of a large number of volatile components, which lead to oxygen consumption, the combustion rate of fixed carbon is zero. With the completion of the precipitation of volatile components, the combustion rate of fixed carbon gradually rises and peaks at ∼7.5 m. As the combustion continues, the combustion rate of fixed carbon gradually decreases and complete combustion occurs at ∼11.5 m.

Figure 4 shows the flue-gas temperature and velocity distribution at the top of the bed. Evidently, in the 0−3 m section, only the evaporation of water in the garbage, the garbage did not catch fire and burn, and the flue-gas temperature is low. At 3 m, due to the precipitation of volatile

https://doi.org/10.1021/acsomega.3c10104
ACS Omega 2024, 9, 14297−14309

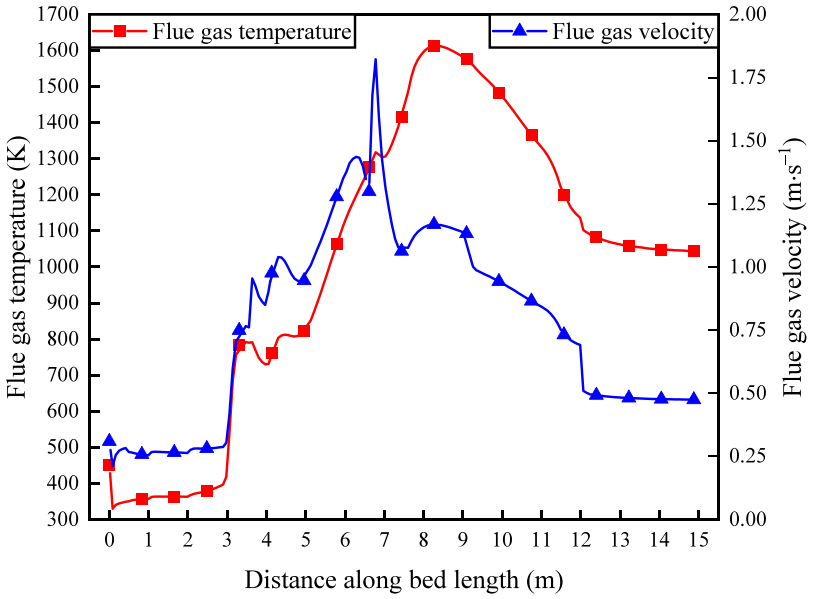

Figure 4. Flue-gas temperature and velocity distribution diagram at the top of the bed.

matter and intense combustion, the temperature and velocity of the flue gas rapidly increase. Combining these results with those shown in Figure 3 demonstrates that at 6.7 m, because of the precipitation of a large number of volatile compounds, the smoke velocity maximizes. Further, as the precipitation rate of volatile compounds decreases, the speed of smoke also gradually decreases. The peak temperature of 1613.38 K occurs at 8.3 m, and according to Figure 3, it is in the stage of fixed carbon combustion. As the fixed carbon combustion rate decreases, the flue-gas temperature and velocity also gradually decrease, and after the end of the combustion, the flue-gas temperature and velocity tend to stabilize.

Figure 5 shows the distribution of flue-gas components at the top of the bed. In the 0−3 m section, the moisture in the flue gas mainly originates from the evaporation of water from the garbage. At 3 m, the moisture content in the flue gas increases owing to the combustion of volatile components, which leads to the generation of water, and combustion leads to a high flue-gas temperature, which accelerates the evaporation of water in the garbage. CH_4 in the flue gas mainly arises from the volatile release; after 7.5 m, CO in the flue gas originates from the incomplete combustion of fixed carbon, while CO in the flue gas in the section from 3 to 7.5 m can be attributed to the volatile release and incomplete combustion of a small proportion of fixed carbon.

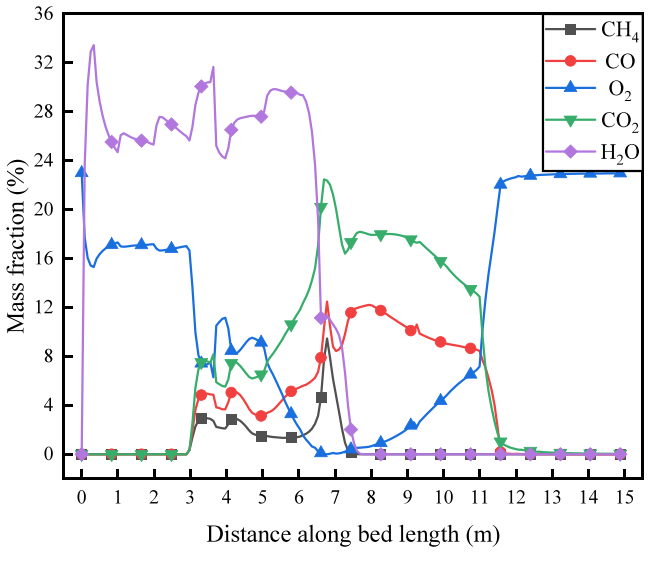

Figure 5. Distribution of flue-gas components at the top of the bed.

The temperature distribution in the center section of the waste incinerator is depicted in Figure 6a, and Figure 6b shows the temperature cloud diagram of the x = 3 m section. Figure 6a,b indicates that the high-temperature region is mainly distributed in the middle section of the grate and at the mouth of the incinerator throat, and the high-temperature region in the middle section of the grate is mainly formed by the combustion of fixed carbon in the garbage bed. Further, considerable secondary wind is injected into the mouth of the throat, resulting in the injection of a large amount of oxygen, and the combustible gases, such as CH_4 and CO, violently burn under the action of the secondary wind, releasing a large amount of heat, leading to a high flue-gas temperature in the region. As the flue gas flows, heat is constantly transferred to the boiler's water−cooled wall, resulting in a gradual decrease in the temperature of the furnace's flue gas with the direction of flue-gas flow.

The flue-gas flow field in the waste incinerator is shown in Figure 6c, which reveals that the flue-gas flow rate is high near the back wall and the flue-gas velocity is high at the mouth of the throat owing to the injection of secondary wind and narrowing of the flow cross section. At the upper part of the throat opening against the back wall, an increase in the runner width causes significant flue-gas reflux. At the top flue bend, flue-gas reflux occurs after the bend, and the flue gas is biased toward the back side of the flue. Figure 6d shows the flue-gas trace diagram, which shows the flue gas in the throat under the action of the secondary wind in the flue-gas combustible components of intense combustion; the flue-gas temperature rises rapidly. After the flue gas enters the flue from the hearth, more flue gas flows toward the back wall, resulting skewing of the high-temperature region toward the back wall.

https://doi.org/10.1021/acsomega.3c10104
ACS Omega 2024, 9, 14297−14309

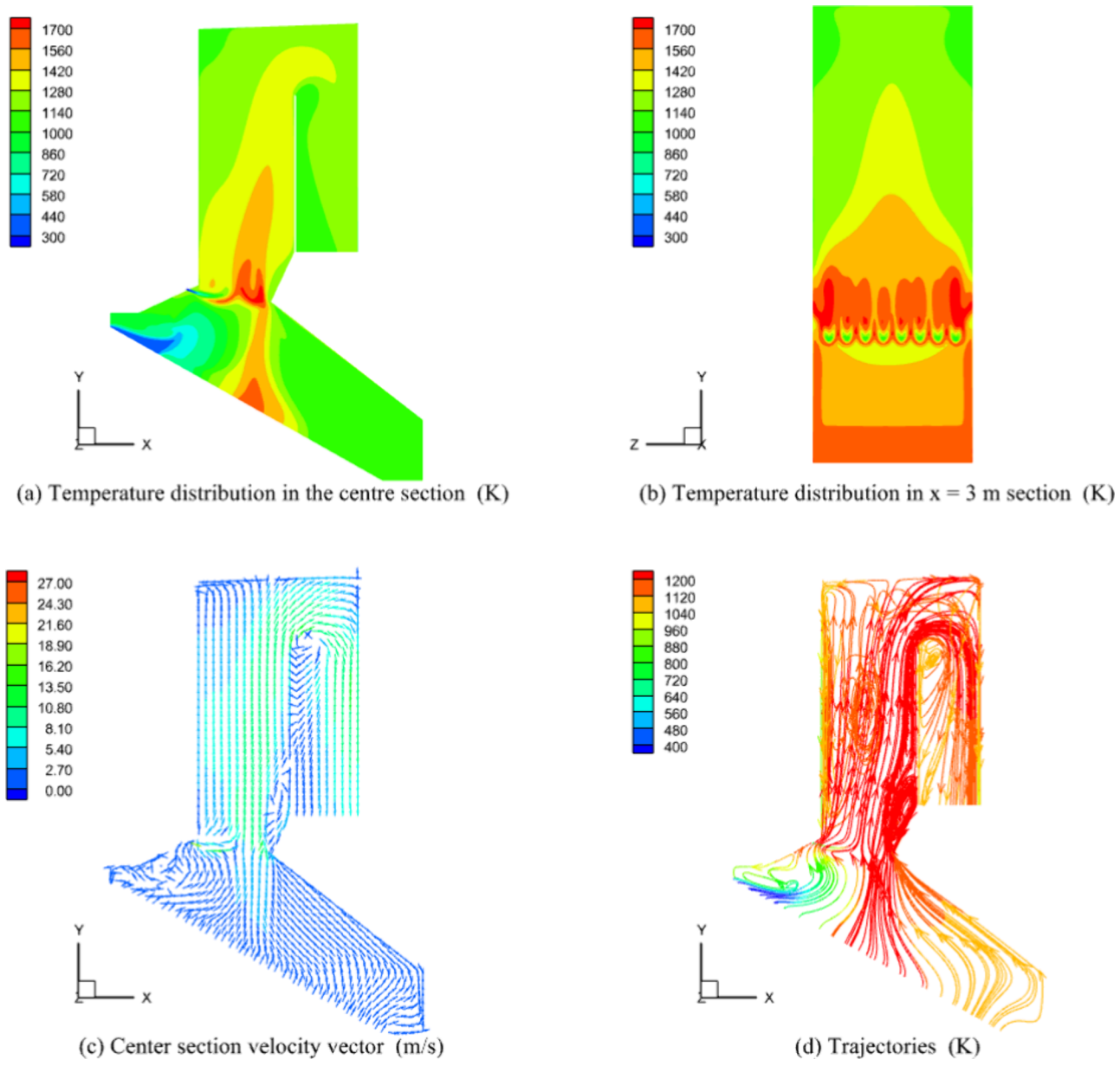

Figure 6. Temperature distribution and velocity distribution graph. Temperature distribution in center section (a). Temperature distribution in x = 3 m section (b). Velocity vector diagram of the center section (c). Trace map of the center section (d).

Table 5 compares the measured and simulated temperature values recorded during the actual operation of the incinerator

Table 5. Comparison of the Measured and Numerically Simulated Values

	T1	T2	T3
numerical simulation/K	1294.09	1227.15	1188.64
measured/K	1239.93	1263.40	1249.23
relative error/%	4.37%	−2.87%	−4.85%

in the waste-to-energy power plant. The locations of the temperature measurement points are shown in Figure 7. Evidently, the relative errors of the three temperature measurement points are 4.37, −2.87, and −4.85%, and the relative errors are less than 5%, indicating that the model has good reliability.

4.2. Effect of Blending Ratio on Bed Combustion.

Municipal solid waste is subjected to different collection seasons, collection and transportation areas, and changes in moisture content, resulting in an unstable calorific value of the waste entering the furnace. Therefore, when simulating the combustion of high moisture−content garbage in the grate furnace, some biomass with a high calorific value is mixed, and the influence of different mixing ratios on the temperature and velocity fields of the furnace is evaluated. Figure 8 shows the moisture evaporation rate, volatile release rate, fixed carbon combustion rate, and flue-gas temperature distribution at the top of the bed. The waste undergoes four processes: drying, pyrolysis, combustion, and combustion exhaustion on the incinerator grate.

Figure 8a shows that the evaporation rates of different blending ratios first decrease and then increase, and the rate maximizes in the combustion grate section because of the release of a large amount of heat from intense combustion,

https://doi.org/10.1021/acsomega.3c10104
ACS Omega 2024, 9, 14297−14309

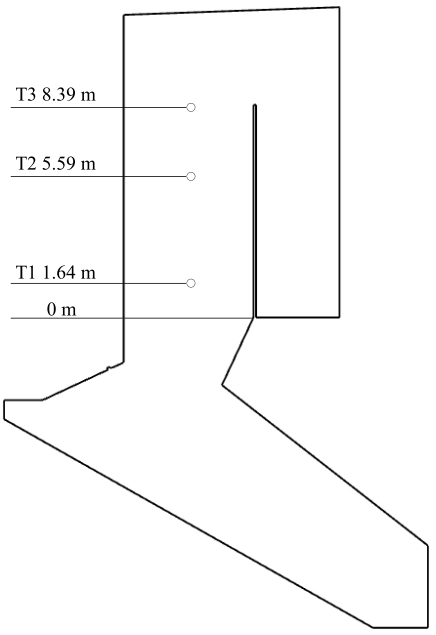

Figure 7. Schematic showing the temperature measurement points.

leading to accelerated precipitation of water. Different blending ratios of fuel moisture content are larger, in the drying grate section, the water evaporation rate with the blending ratio changes are not obvious. In the combustion grate section, as the blending ratio of biomass increases, the water content of the garbage decreases, the volatile matter increases, the garbage catches fire and burns to release a large amount of heat, and the water evaporation process is completed earlier.

As can be seen from Figure 8b, the precipitation rate of volatile matter shows a trend of increasing, then decreasing, then increasing, and reaching the peak, the water content of the garbage is high, and a large amount of heat released by the garbage after it catches fire and burns is absorbed by the water; thus, the water evaporation rate is accelerated and the precipitation rate of the volatiles decreases, but with the completion of the evaporation of the water, the precipitation rate of the volatiles increases rapidly to the peak value and completes the precipitation process. With the increase of blending ratio, the proportion of volatile matter in the fuel increases, and a large amount of volatile matter releases heat after combustion, accelerating the precipitation process of volatile matter, so the precipitation of volatile matter is completed earlier, and the precipitation of volatile matter is completed in the combustion grate section.

Figure 8c shows that, as combustion proceeds, the coke starts to ignite after the volatile release of the upper layer of waste, releasing a large amount of heat to accelerate the precipitation of volatile components, but a large amount of volatile release, wrapped around the coke particles, hinders the diffusion of oxygen to the coke, so the burning rate of the coke appears to be peaks and valleys. At the end of combustion, the burning rate of fixed carbon gradually decreases. Due to the high content of fixed carbon in biomass, the combustion of fixed carbon burns out earlier as the mixing ratio increases.

Figure 8d shows that due to the increase in the blending ratio, the ignition combustion of the fuel is advanced, the increase in the flue-gas temperature at the top of the bed is subsequently advanced, and the moisture evaporation process of the waste controls the whole bed combustion to a large

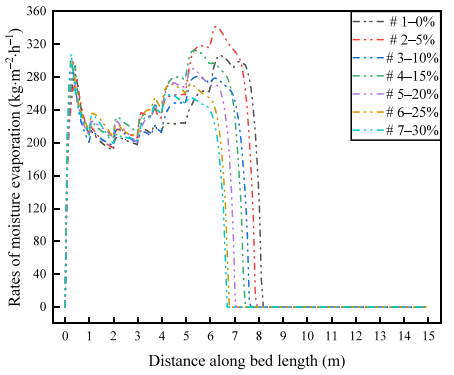

(a) Rates of moisture evaporation

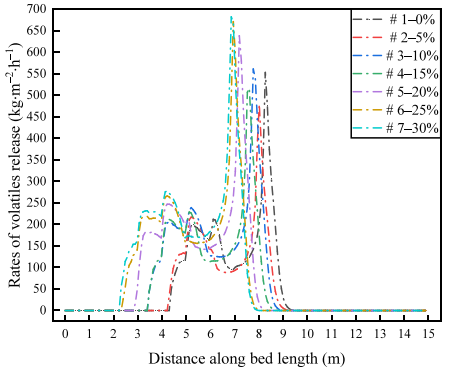

(b) Rate of volatiles release

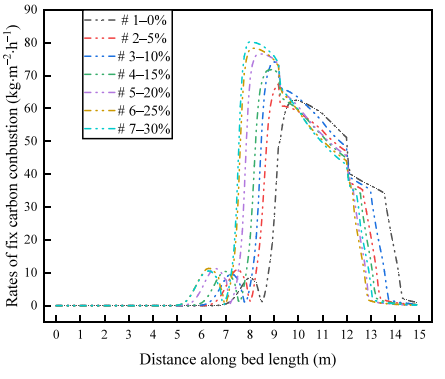

(c) Rates of carbon combustion

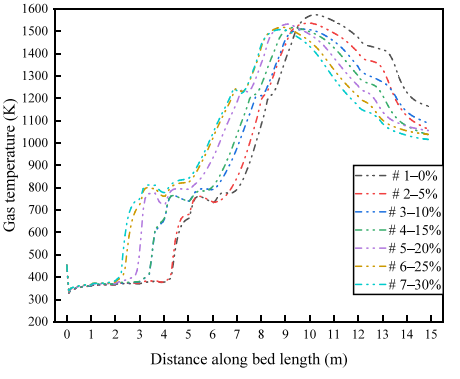

(d) Flue-gas temperature at the top of the bed

Figure 8. Water evaporation rate, volatilization rate, fixed carbon combustion rate, and flue-gas temperature distribution at the top of the bed. (a) Rates of moisture evaporation, (b) rate of volatiles release, (c) rates of carbon combustion, and (d) flue-gas temperature at the top of the bed.

https://doi.org/10.1021/acsomega.3c10104
ACS Omega 2024, 9, 14297−14309

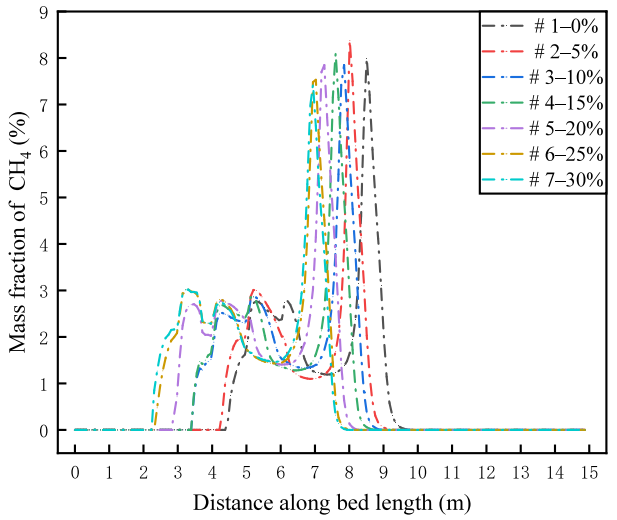

(a) Mass fraction of CH_4

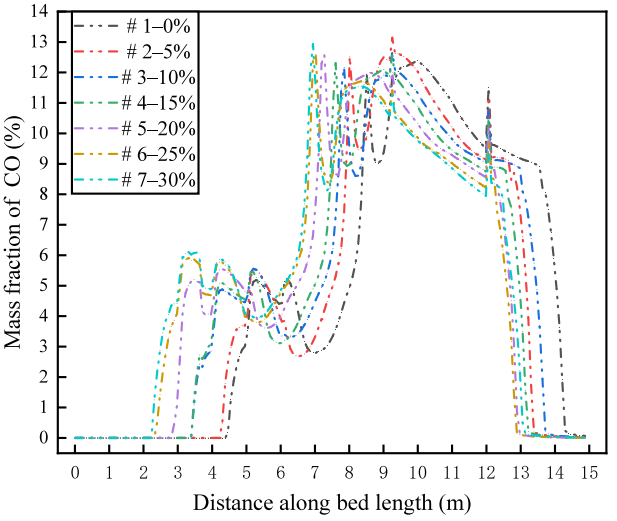

(b) Mass fraction of CO

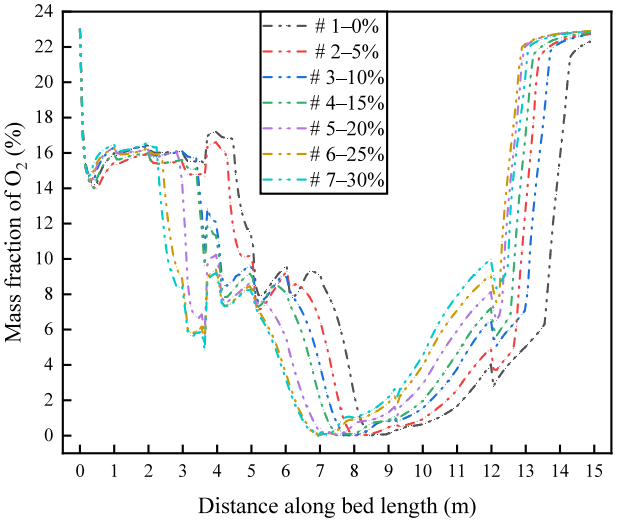

(c) Mass fraction of O_2

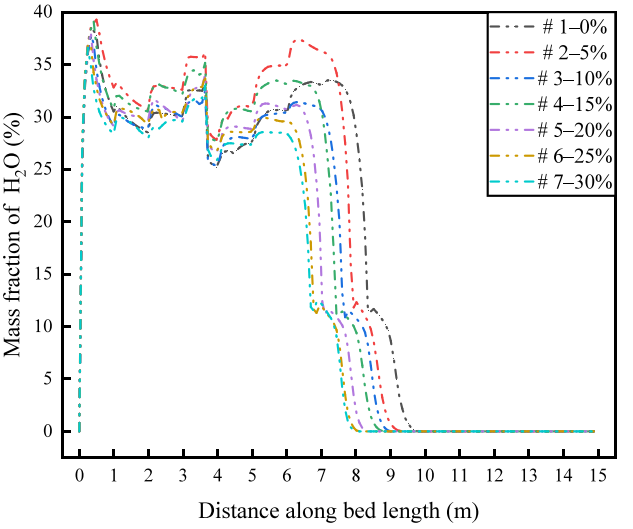

(d) Mass fraction of H_2O

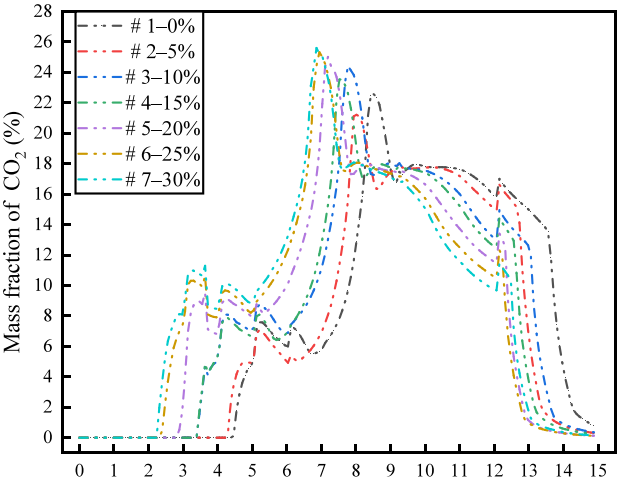

(e) Distance along bed length (m)

Figure 9. Distribution of CH_4, CO, O_2, H_2O, and CO_2 in the flue-gas components at the top of the bed. (a) Mass fraction of CH_4. (b) Mass fraction of CO. (c) Mass fraction of O_2. (d) Mass fraction of H_2O (e) Mass fraction of CO_2.

https://doi.org/10.1021/acsomega.3c10104
ACS Omega 2024, 9, 14297−14309

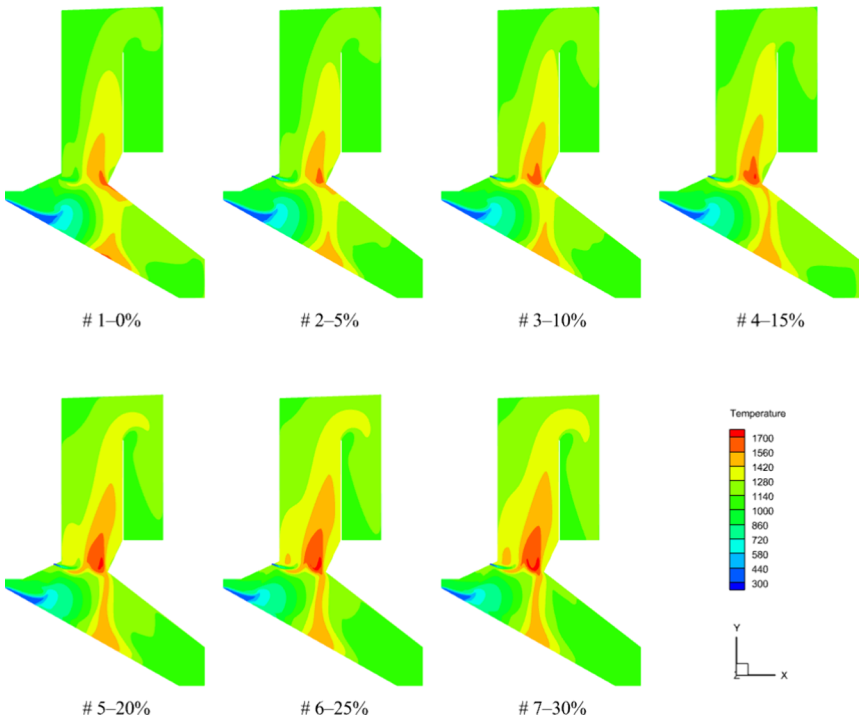

Figure 10. Temperature distribution in the central section under different working conditions (K).

extent. The combustion lag of 0 and 5% blending ratios and a decrease in the air distribution ratio in the burnout grate section are observed; therefore, the peak temperatures of these two conditions appear in the burnout grate section, and the peak temperatures are higher than those of the other conditions.

Figure 9 shows the distributions of CH_4, CO, O_2, H_2O, and CO_2 in the flue-gas components at the top of the bed. Figure 9a shows that the mass fraction of CH_4 in the flue gas has the same trend with the volatile analyzed rate in Figure 8b, which is due to the fact that the CH_4 in the flue gas mainly comes from the release of volatile components. Figure 9b shows that the mass fraction of CO in the flue gas changes similarly to the volatile analysis rate in the 2.2−8.5 m section, because the CO in the flue gas comes from the precipitation of volatile matter and the incomplete combustion of the fixed carbon, and with the completion of the volatile matter precipitation after 8.5 m, the CO in the flue gas comes from the incomplete combustion of coke, and with the completion of the coke combustion the mass fraction of CO in the flue gas also decreases to 0.

Figure 9c shows that in the drying grate section the mass fraction of O_2 decreases due to the large amount of water evaporation and the large amount of H_2O in the flue gas. As combustion proceeds, the released volatile matter burns and consumes a large amount of O_2, resulting in a rapid decrease in the mass fraction of O_2 in the flue gas, while in the ash combustion grate section, due to the gradual exhaustion of the combustible components in the bed material, the mass fraction of O_2 in the flue gas begins to gradually increase.

Figure 9d shows that in the drying grate section, the water evaporates a large amount and the mass fraction of H_2O in the flue gas is higher, but as the evaporation proceeds, the water content in the bed material decreases, so the mass fraction of H_2O in the flue gas also decreases gradually; however, with the release of heat from the bed material ignition and combustion, the mass fraction of H_2O in the flue gas gradually rises. In the combustion grate section, the mass fraction of H_2O in the flue gas decreased due to the increase of the primary air volume, but a large number of volatile components burned to produce water, which led to a rise in the mass fraction of H_2O in the flue gas, and with the completion of the release of the volatile components, the mass fraction of H_2O in the flue gas decreases to 0.

Figure 9e shows that the trend of the mass fraction of CO_2 in the flue gas is consistent with that of CO, which is due to the fact that CO_2 comes from the combustion of volatiles and the combustion of fixed carbon. In summary, the release of CH_4, CO, CO_2, etc., in the flue gas at the top of the bed is carried out with the increase of biomass blending ratio, and the combustion is completed earlier due to the increase of biomass blending ratio, the relative decrease of fuel water content, and the increase of calorific value. Thus, the process of water evaporation from the waste controls the combustion throughout the bed to a large extent.

4.3. Effect of Blending Ratio on Incinerator Temperature. Figure 10 shows the cloud diagram of the temperature distribution in the center section of the furnace chamber for different working conditions. With the increase of blending ratio, the high-temperature region at the mouth of the throat gradually increases, and the flue-gas temperature at the exit of the furnace chamber increases. As the blending ratio increases, the total volatile matter in the fuel rises because of the high volatile matter content in the biomass. The combustible gases produced by the increased volatile fraction of the fuel react violently at the throat when mixed with the secondary air, resulting in an increase in temperature at the throat. The high-temperature region at the rear arch is shifted forward, causing ignition and combustion of the fuel on the bed. Therefore, a certain proportion of blended biomass can reduce the erosion of high temperature on the rear arch and improve the stability of combustion.

https://doi.org/10.1021/acsomega.3c10104
ACS Omega 2024, 9, 14297−14309

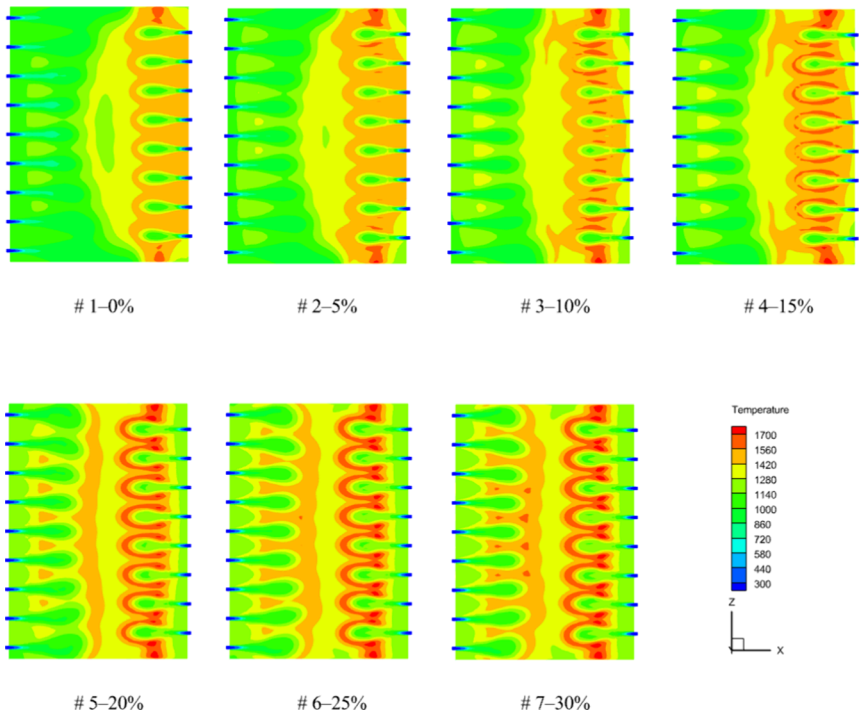

Figure 11. Secondary air outlet cross-sectional temperature distribution (K).

Figure 11 shows the temperature distribution cloud diagram of the cross-section of the secondary air outlet, from which it can be seen that with the increase of biomass blending ratio, the temperature of the secondary air region gradually increases, the high-temperature region gradually increases, and the high-temperature region gradually moves to the center. The source is that that the biomass mixing ratio increases, the more combustible gas generated by the bed combustion, the more intense combustion in the secondary air injection. The high-temperature region in the middle of the furnace can reduce the high-temperature erosion of the water-cooled wall.

Various conditions of the incinerator outlet temperature are shown in Figure 12. The mixing ratio increases from 0 to 30%, and the outlet temperature increases from 1021 to 1105 K, which indicates an increase of 84 K. When the mixing ratio increases from 15 to 20%, the export temperature difference maximizes.

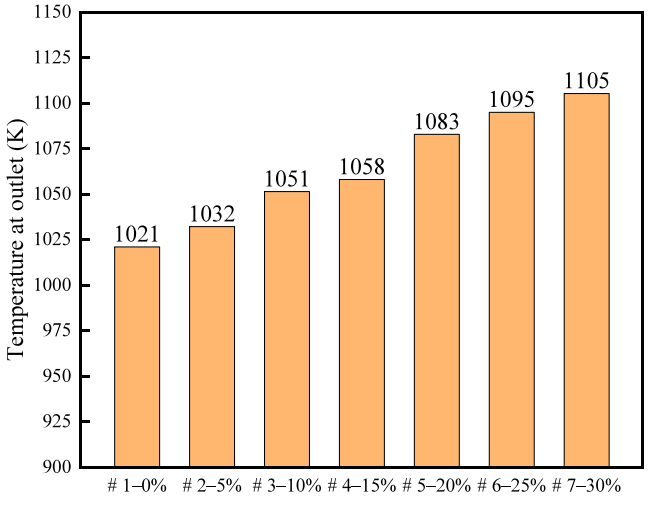

Figure 12. Outlet temperature for different conditions.

Figure 13 shows the average temperature distribution along the height direction of the incinerator under different working

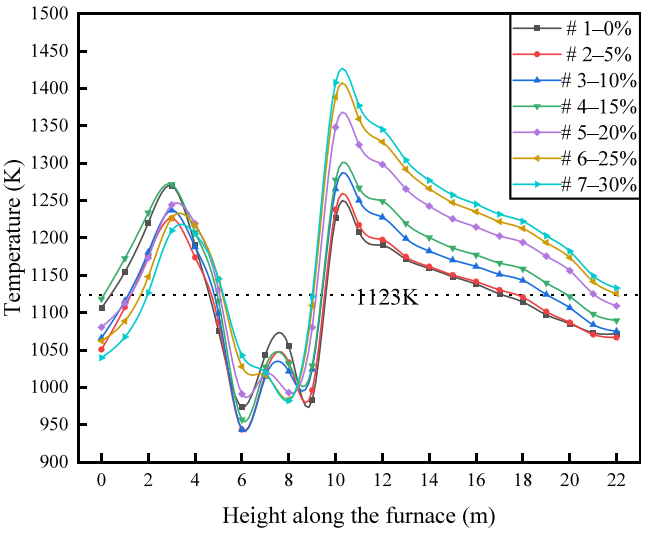

Figure 13. Average temperature along the height of the incinerator.

conditions. Evidently, the temperature trend along the height direction is basically the same for different mixing ratios. In the 4−10 m section, the average temperature decreases because of the injection of secondary air. However, with complete mixing of the injected secondary air and flue gas, CH_4 and CO in the flue gas violently combust and release a large amount of heat, which rapidly increases the temperature and the temperature peaks at 10 m. With the flow of flue gas, the high-temperature flue gas continuously exchanges heat with the water-cooled wall, and the temperature gradually decreases. The peak

https://doi.org/10.1021/acsomega.3c10104
ACS Omega 2024, 9, 14297−14309

temperature of the incinerator increases from 1227 to 1408 K as the blending ratio gradually increases.

Figure 14 shows the flue-gas velocity distribution along the incinerator height direction. This distribution profile indicates

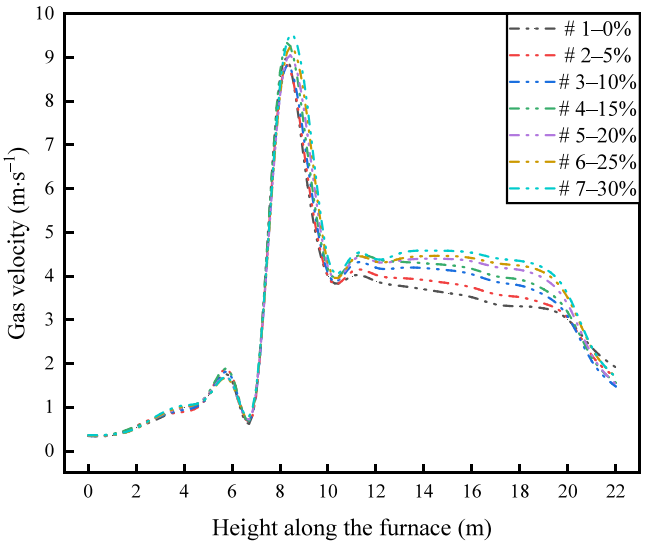

Figure 14. Flue-gas velocity distribution along the incinerator height direction.

that the flue-gas velocity is maximized at 8 m because of the considerable secondary wind injection in this region, resulting in a high flue-gas flow velocity in this region. To effectively reduce the generation of dioxin, the flue gas must stay in the high-temperature region (more than 1123 K) for more than 2 s. These results collectively with those shown in Figure 13 indicate that the residence times of the flue gas in cases 1−4 are 1.62, 1.83, 1.79, and 1.93 s, respectively, which do not meet the requirement of staying in the high-temperature region for more than 2 s. Therefore, cases 1−4 cannot effectively minimize the generation of dioxin. The residence time of the flue gas in the high-temperature region of working conditions 5−7 are 2.39, 2.69, and 2.62 s, respectively, all of which satisfy the residence time of above 2 s and can effectively reduce the generation of dioxin.[25]

4.4. Effect of Blending Ratio on NO_x Emission. NO_x, one of the pollutants produced during waste incineration, is the main factor causing acid rain, include mainly NO and NO_2, with NO accounting for 95% and NO_2 for 5% of the NOx produced by combustion, and SNCR is widely used in power plants for flue-gas NO_x removal. Figure 15 shows the export NO_x concentration under different blending ratios when SNCR ammonia injection denitrification is not used. Evidently, the export NO_x concentration increases gradually as the blending ratio increases. Combined with Table 1, it can be seen that the nitrogen content in the low-quality waste is 1.46%, and the nitrogen content in the biomass is 3.39%, which increases with the increasing blending ratio of the biomass. Further, the increase in the blending ratio results in a decrease in the moisture content of the fuel, while the calorific value of the fuel entering the furnace increases along with expansion of the high-temperature region in the furnace, an increase in the residence time of the flue gas in the high-temperature region, and the generation of thermodynamic NO_x. Therefore, the export NO_x concentration increases with the increasing blending ratio of SNCR injection ammonia denitrification,

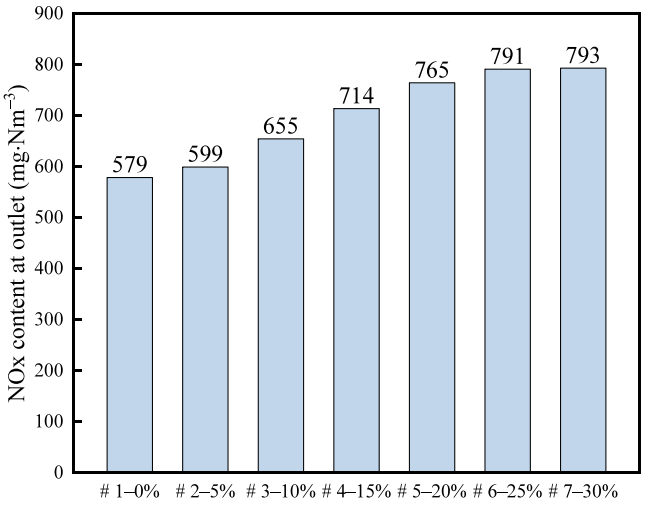

Figure 15. Outlet NOx concentration without SNCR (11% O_2).

whereas the NO_x concentration at the outlet increases with the decreasing blending ratio. To sum up, the NO_x concentration increases with an increasing blending ratio.

Figure 16 shows the NO_x concentration at the exit under different normalized stoichiometric ratios. With the increase in

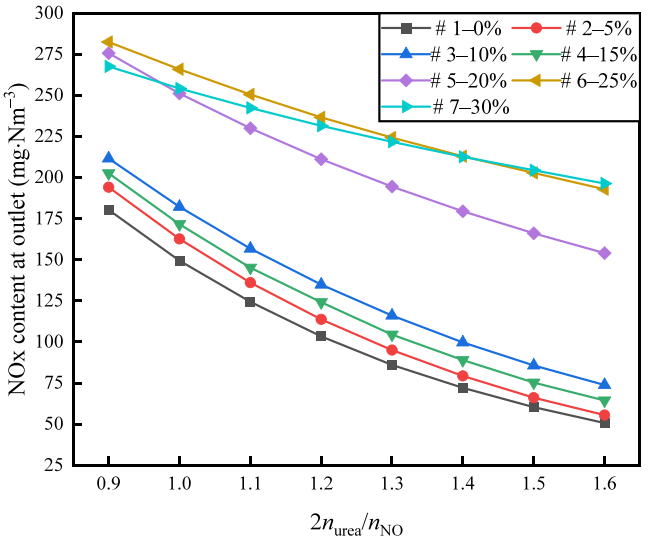

Figure 16. NO_x concentration at the outlet with different normalized stoichiometric ratios (11% O_2).

normalized stoichiometric ratio, the NO_x concentration at the exit of different blending ratios decreases; the urea injected into the chamber of the SNCR increases; the amount of NH_3 produced via pyrolysis increases and the contact area between the NH_3 molecules with NO_x increases,[26] resulting in a decrease in the outlet NO_x concentration. As the biomass blending ratio increases to 20%, the SNCR denitrification effect weakens. However, when the normalized stoichiometric ratio increases, the outlet NO_x concentration−deterioration rate reduces because of the increasing biomass blending ratio. The SNCR spraying area temperature is too high, resulting in oxidation of certain NH_3 molecules, which in turn weakens the denitrification effect.

Figure 17 shows the NH_3 concentration at the outlet for different normalized stoichiometric ratios. An increase in the

https://doi.org/10.1021/acsomega.3c10104
ACS Omega 2024, 9, 14297−14309

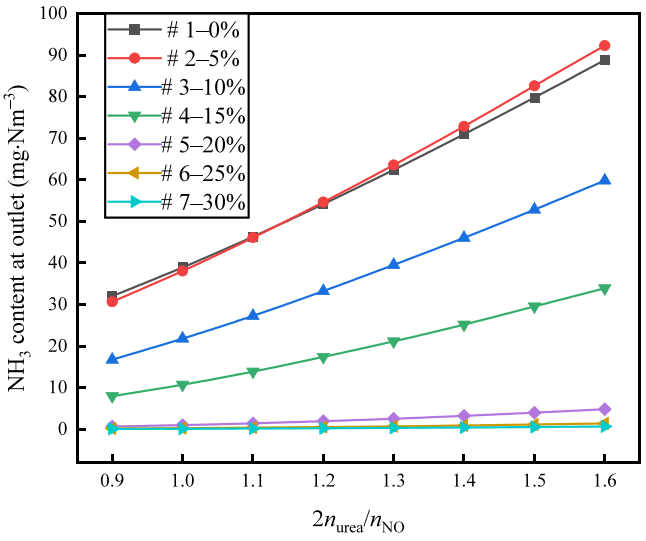

Figure 17. Outlet NH_3 concentration at different normalized stoichiometric ratios (11% O_2).

normalized stoichiometric ratio for different biomass blending ratios increases the outlet NH_3 concentration owing to the inhomogeneous mixing of NH_3 and NO_x. As the biomass blending ratio increases to 20%, the temperature of the SNCR spraying area increases and a fraction of NH_3 is oxidized, which results in a low export NH_3 concentration at three biomass blending ratios of 20, 25, and 30%. Combining these results with those shown in Figure 16 reveals that the outlet NO_x concentration of condition # 5%−20% is 230.08 mg/Nm^3 at a normalized stoichiometric ratio of 1.1; this concentration meets the nitrogen-oxide emission standard (less than 250 mg/Nm^3). In addition, the outlet NH_3 concentration is 1.44 mg/Nm^3, and the normalized stoichiometric ratio is greater than 1.1 to meet the emission standard for both conditions # 6−25% and # 7−30%. From the viewpoint of saving the cost of ammonia spraying, condition # 5−20% is the best one.

5. CONCLUSIONS

In this study, we employed FLIC and Fluent to numerically simulate the effect of biomass blending on furnace temperature, pollutant generation, and SNCR denitrification of a 600 t/day waste incinerator during the treatment of low calorific−value waste. The results showed that an increase in the biomass blending ratio resulted in a gradual decrease in the water content of the fuel in the furnace, an increased calorific value, and a gradual increase in the maximum temperature of the furnace chamber from 1227 to 1408 K. On the contrary, the increasing biomass blending ratio increased the amount of NO_x produced from 579 to 793 mg/Nm^3. The calculated residence time of the flue gas in the high-temperature region was 1.62 s during the burning of low-quality garbage. Evidently, a biomass blending ratio of >20% resulted in a flue-gas residence time of 2.39 s in the high-temperature region. This residence time effectively inhibited the generation of dioxin. By contrast, a biomass blending ratio of 20% and molar ammonia/nitrogen ratio of 1.1 collectively resulted in an outlet NO_x concentration of 230.08 mg/Nm^3, which aligned with the NO_x emission standard of less than 250 mg/Nm^3.

AUTHOR INFORMATION

Corresponding Author

Dehong Gong − *School of Electrical Engineering, Guizhou University, Guiyang, Guizhou 550025, China*; Email: dhgong@gzu.edu.cn

Authors

Zhengguang Huang − *School of Electrical Engineering, Guizhou University, Guiyang, Guizhou 550025, China*; orcid.org/0009-0001-5893-3466

Changyang Peng − *POWERCHINA GUIZHOU ENGINEERING CO.,LTD., Guiyang, Guizhou 550003, China*

Jiandong Chen − *POWERCHINA GUIZHOU ENGINEERING CO.,LTD., Guiyang, Guizhou 550003, China*

Jie Luo − *POWERCHINA GUIZHOU ENGINEERING CO.,LTD., Guiyang, Guizhou 550003, China*

Yuanyuan Xu − *School of Electrical Engineering, Guizhou University, Guiyang, Guizhou 550025, China*

Lang Yang − *School of Electrical Engineering, Guizhou University, Guiyang, Guizhou 550025, China*

Complete contact information is available at: https://pubs.acs.org/10.1021/acsomega.3c10104

Notes

The authors declare no competing financial interest.

ACKNOWLEDGMENTS

The research was sponsored by the Guizhou Province Science and Technology Support Program (QIANKEHE Support [2022] General 018).

REFERENCES

(1) China, N. B. S. P. s. R. o. 2022 *China Statistical Yearbook*. 2022.

(2) Sun, Y.; Qin, Z.; Tang, Y.; Huang, T.; Ding, S.; Ma, X. Techno-environmental-economic evaluation on municipal solid waste (MSW) to power/fuel by gasification-based and incineration-based routes. *Journal of Environmental Chemical Engineering* **2021**, *9* (5), No. 106108.

(3) Shah, A. V.; Srivastava, V. K.; Mohanty, S. S.; Varjani, S. Municipal solid waste as a sustainable resource for energy production: State-of-the-art review. *Journal of Environmental Chemical Engineering* **2021**, *9* (4), No. 105717.

(4) Liu, Q.; Sun, Y. H.; Kou, W.; Cao, Y. X.; Wang, X. M.; Liu, Z. W.; Zhang, H. Compositions analysis and anaerobic digestion characteristics on seasonal municipal solid waste. *Chin. J. Environ. Eng.* **2013**, *7* (11), 4507−4512.

(5) Sun, R.; Ismail, T. M.; Ren, X.; El-Salam, M. A. Influence of simulated MSW sizes on the combustion process in a fixed bed: CFD and experimental approaches. *Waste Manag.* **2016**, *49*, 272−286.

(6) Hoang, Q. N.; Van Caneghem, J.; Croymans, T.; Pittoors, R.; Vanierschot, M. A novel comprehensive CFD-based model for municipal solid waste incinerators based on the porous medium approach. *Fuel* **2022**, *326*, No. 124963.

(7) Wissing, F.; Wirtz, S.; Scherer, V. Simulating municipal solid waste incineration with a DEM/CFD method−Influences of waste properties, grate and furnace design. *Fuel* **2017**, *206*, 638−656.

(8) Gu, T.; Ma, W.; Berning, T.; Guo, Z.; Andersson, R.; Yin, C. Advanced simulation of a 750 t/d municipal solid waste grate boiler to better accommodate feedstock changes due to waste classification. *Energy* **2022**, *254*, No. 124338.

(9) Yan, M.; Tian, X.; Yu, C.; Zhou, Z.; Hantoko, D.; Kanchanatip, E.; Khan, M. S. Influence of multi-temperature primary air on the

https://doi.org/10.1021/acsomega.3c10104
ACS Omega 2024, 9, 14297−14309

characteristics of MSW combustion in a moving grate incinerator. *J. Environ. Chem. Eng.* **2021**, *9* (6), No. 106690.
(10) Yang, X.; Yu, Z. S.; He, Y. R.; Bin, Y. H.; Ma, X. Q. Numerical simulation of municipal domestic waste blending with combustion of high calorific value industrial solid waste inwaste incineration furnace. *Clean Coal Technol.* **2023**, *29* (9), 1.
(11) Zeng, X. H.; Ma, X. Q.; Liao, Y. F.; Wang, H. C. Numerical simulation of Co-combustion of Sludge in a 900 t/d Waste Incinerator. *J. Eng. Thermophys.* **2020**, *41* (9), 2324−2332.
(12) Hu, Z.; Jiang, E.; Ma, X. Numerical simulation on operating parameters of SNCR process in a municipal solid waste incinerator. *Fuel* **2019**, *245*, 160−173.
(13) Huang, Z. G.; Gong, D. H.; Xu, Y. Y.; Yang, L. Experimental study on release chanracteristics of tar productsfrom tobacco stem pyrolysis. *Acta Energ. Sol. Sin.* **2023**, 1−8.
(14) Yang, Y. B.; Yamauchi, H.; Nasserzadeh, V.; Swithenbank, J. Effects of fuel devolatilisation on the combustion of wood chips and incineration of simulated municipal solid wastes in a packed bed☆. *Fuel* **2003**, *82* (18), 2205−2221.
(15) Chen, J.; Tang, J.; Xia, H.; Yu, W.; Qiao, J. Modelling the furnace temperature field of a municipal solid waste incinerator using the numerical simulation and the deep forest regression algorithm. *Fuel* **2023**, *347*, No. 128511.
(16) Yang, Y. B.; Goh, Y. R.; Zakaria, R.; Nasserzadeh, V.; Swithenbank, J. Mathematical modelling of MSW incineration on a travelling bed. *Waste management* **2002**, *22* (4), 369−380.
(17) Yang, Y. B.; Phan, A. N.; Ryu, C.; Sharifi, V.; Swithenbank, J. Mathematical modelling of slow pyrolysis of segregated solid wastes in a packed-bed pyrolyser. *Fuel* **2007**, *86* (1−2), 169−180.
(18) Wang, H.; Jin, H.; Yang, Z.; Deng, S.; Wu, X.; An, J.; Sheng, R.; Ti, S. CFD modeling of flow, combustion and NOx emission in a wall-fired boiler at different low-load operating conditions. *Applied Thermal Engineering* **2024**, *236*, No. 121824.
(19) Yang, Y. C. *Numerical Simulation of Incineration Optimization and Lower Nitrogen Technology in Municipal Solid Waste Incinerator*. 2022. https://link.cnki.net/doi/10.27151/d.cnki.ghnlu.2022.000992.
(20) Zhao, Y.; Feng, J.; Chen, Y.; Fan, H.; Bai, W. Thermal process and NO emission reduction characteristics of a new-type coke oven regenerator coupled with SNCR process. *Fuel* **2021**, *305*, No. 121510.
(21) Rota, R.; Antos, D.; Zanoelo, E. F.; Morbidelli, M. Experimental and modeling analysis of the NOxOUT process. *Chem. Eng. Sci.* **2002**, *57* (1), 27−38.
(22) Brouwer, J.; Heap, M. P.; Pershing, D. W.; Smith, P. J. A model for prediction of selective noncatalytic reduction of nitrogen oxides by ammonia, urea, and cyanuric acid with mixing limitations in the presence of CO. *Elsevier* **1996**, *26*, 2117−2124.
(23) Ke, X.; Yao, Y.; Huang, Z.; Zhang, M.; Lyu, J.; Yang, H.; Zhou, T. Prediction and minimization of NOx emission in a circulating fluidized bed combustor: Improvement of bed quality by optimizing cyclone performance and coal particle size. *Fuel* **2022**, *328*, No. 125287.
(24) Bo, L.; Han, K. H.; Qi, J. H.; Liu, S. L.; Ma, C. G. Numerical Simulation of Pulsed Jet Denitrification for SNCR. *Proc. CSEE* **2023**, *43* (07), 2771−2781. From Cnki.
(25) Lin, T.; Liao, Y.; Dai, T.; Ma, X. Investigation on co-disposal technology of sludge and municipal solid waste based on numerical simulation. *Fuel* **2023**, *343*, No. 127882.
(26) Xu, Y. Y.; Gong, D. H.; Deng, C. J.; Wang, K.; Wang, J. C.; Ye, Z. Q.; Huang, Z. G.; Yang, L. Interaction effect of inlet parameters and reaction temperature on denitration performance of SCR reactor. *Chin. J. Environ. Eng.* **2023**, 1−11.

https://doi.org/10.1021/acsomega.3c10104
ACS Omega 2024, 9, 14297−14309